Computer-Aided Design 108 (2019) 1–11

Contents lists available at ScienceDirect

Computer-Aided Design

journal homepage: www.elsevier.com/locate/cad

# Texture-guided generative structural designs under local control[☆]

Jingqiao Hu[1], Ming Li[*], Shuming Gao[2]

*State Key Laboratory of CAD&CG, Zhejiang University, Hangzhou, China*

ARTICLE INFO

*Keywords:*
Generative design
Texture-guided
Topology optimization
Physics-adaptive regulator
Local feature control

ABSTRACT

A novel generative design approach is developed in this study, which produces a mechanically optimized topological design while simultaneously mimicking an input exemplar texture. The textures are believed embedding certain functional information intrinsic to these objects. Designing objects similar to these textures will not only maintain such functions within the design but also widely expand the design space to explore more design options. However, simple textural replications or reconstructions cannot produce expected designs as an ideal structure has to adapt to the variations of the complex stress distributions caused by external loadings. On the other hand, a simple topology optimization formulation under a single *global* similarity constraint may produce undesirable structures exhibiting geometric disconnections or boundary protrusions.

Due to these considerations, the proposed approach carefully formulates the problem as a classical topological compliance minimization problem under *block-wise* similarity constraints between the target design and an input texture. In addition, a novel *physics-adaptive regulator* is also proposed, which fine-tunes the block similarity according to its per-element compliances. Ultimately, we can create a set of design options both physically optimized and geometrically smooth for generative design. Extensive numerical results were also tested to demonstrate the approach's performance.



## 1. Introduction

The recent fast development of addictive manufacturing technologies has allowed designers to directly fabricate structures of almost arbitrary shapes, and greatly extends the design space. It on the other hand raises the challenging issue on reliable structure design for such complex structures, which is almost impossible to handle successfully even for an experienced designer. Designers have thus been exploring generative design as a new way of creating industrial designs [1]. With generative design, the designer sets up a high-level design objective and constraints, and let computers automatically find various design options best fitting their criteria. These options may spark creative ideas or even provide the first draft toward the final design.

Generative design reshapes the design viewpoints. Actually, traditional CAD technologies mainly focus on providing a professional design tool so that the design expert can create an object step by step based on their professional experience. In this process, the expert is in charge of the design, and it usually involves tedious repeated modifications and simulations before reaching the final design. In contrast, generative design incorporates the computational power of modern computing facilities and the intuition and expertise of designers – generating thousands of design options and the designer making the final selection. The importance of generative design has also been recognized and adopted by leading-edge CAD providers, for example AutoCAD recently released a generative design software DreamCatcher [2].

Topology optimization [3,4] is deemed as one of the powerful candidates to realize the concept of generative design. It aims to optimally distribute the materials within a design domain for optimized physical performance under certain design constraints. However, traditional topology optimization approaches are restricted in only providing a very small number of candidate structures, which limits the designers' freedom of choices.

On the other hand, textures are widely found in natural or man-made objects, and are believed embedding certain functional

☆ This paper has been recommended for acceptance by Chennai Guest Editor

* Correspondence to: Room 517, Mengminwei Building, Zijingang Campus, .
*E-mail addresses:* hujingqiao@zju.edu.cn (J. Hu), liming@cad.zju.edu.cn (M. Li), smgao@cad.zju.edu.cn (S. Gao).

1 Room 419, Mengminwei Building, Zijingang Campus.

2 Room 514, Mengminwei Building, Zijingang Campus.

https://doi.org/10.1016/j.cad.2018.10.002
0010-4485/

information intrinsic to these objects [5]. Designing objects similar to these textures will not only have chances to maintain such functions within the design but also widely expand the design space to explore more design options. However, simple textural replications or reconstructions [6–8] cannot produce expected designs as an ideal structure has to adapt to the variations of the complex stress distributions caused by external loadings.

Based on the considerations, we propose in this paper a texture-guided generative structural design approach that tightly couples recent advances on topology optimization [4] and texture synthesis [8]. It automatically creates various design options by locally mimicking input textural images under some controlling parameters for ultimate goal of design space exploration. The proposed approach rigorously formulates the design problem as a topology optimization problem under a set of *block-wise* similarity constraints between the design and the exemplar texture. In addition, a novel *physics-adaptive regulator* is also proposed, which fine-tunes the block similarity according to its per-element compliances. Ultimately, we can create a set of design options both physically optimized and geometrically smooth for generative design, as demonstrated via extensive numerical results.

The study is closely related to the previous excellent work conducted by Martinez et al. [9] on structure and appearance optimization for controllable shape design. Different from the present study on generative design, their work focuses on generating esthetic structures using input textures under certain physical reliability. It consequently takes a global shape similarity as the design target and physical reliability as a constraint. It is able to generate various attracting and reliable structures, but on the other hand leaves much space for performance improvement of the generated structures. It sometime even may produce undesirable structures exhibiting geometric disconnections or boundary protrusions [9]; as will be shown in Section 3. Thus, the approach in [9] is not directly applicable for the purpose of generative design, as studied here. More details on differences between the two approaches will be shown in Sections 3 and 6.

The remainder of the paper is organized as follows. Related work is first discussed in Section 2. After this, the problem on generative structural design is mathematically formulated in Section 3. The numerical details are respectively explained in Sections 4 and 5 on optimization approach and similarity regulation. After demonstrating the numerical examples in Section 6, the paper is concluded in Section 7.

## 2. Related work

Related work on topology optimization and texture synthesis is first discussed in this section.

### 2.1. Topology optimization

Topology optimization aims to find the optimized material distribution within a design domain for structure performance optimization. Most previous approaches relax the problem into a continuous parameter optimization problem using size, density or shape, and then solve it based on traditional Newton-type (gradient-based) or evolutionary optimization algorithms. Classical topology optimization approaches include homogenization [10], density-based method (SIMP, Solid Isotropic Material with Penalization) [11], evolutionary approaches (BESO, Bi-directional Evolutionary Structural Optimization) [12,13], level set [14,15], or techniques in B-spline spaces [16]. The SIMP framework is applied here.

Most previous studies on topology optimization are mainly concerned with certain *physical* objectives and constraints at a prescribed volume budget [4]. Studies on topology optimization problem under geometric constraints are quite very few, and most of them focus on thickness control [17] or shape control [18–21] and seldom consider texture similarity. Recently, including a geometric constraint on self-supporting for addictive manufacturing attracts widely research interests [22–25].

In contrast, the proposed approach aims to generate different shape features from a new point of view using planar texture exemplars via controlling their geometric similarity. Wu et al. [26] recently also proposed a very interesting approach to generating a bone-like structure via including various carefully designed explicit constraints on feature sizes or local volumes. Different from this, the present study focuses on using an input exemplar image to guide the topology optimization results without the huge efforts devoted in designing the control rule, and is applicable to any kind of features.

### 2.2. Texture synthesis

Texture synthesis aims to generate a new 2D or 3D texture from a 2D exemplar image, and is a long-standing topic in image processing and computer graphics [27]. The initial work was based on Markov random fields (MRFs) [6,7]. Later, Kwatra et al. [8] formulated it as an energy minimization problem defined by the difference between the exemplar and design structure/image. A similar strategy is also adopted in the current study. Kopf et al. [28] extended the synthesis from 2D to 3D by sampling on three slices orthogonal to the $x$, $y$, and $z$ axes. However, no physical performance was involved in these studies.

A series of excellent work to synthesize textural structures was recently conducted by Liu and Shapiro [29,30], focusing on random heterogeneous or anisotropic material properties. These approaches are mainly based on reconstruction using two-point correlation functions [31] using statistical material descriptors, and optimized topology was assumed given in advance.

## 3. Problem statement

We aim to generate various 2D structures that exhibit optimized physical performance and simultaneously preserve certain geometric similarity with an exemplar image, as illustrated in Fig. 1. These automatically generated structures can be provided as design candidates for experts to select to ultimately meet the design requirements.

Let $\mathcal{I}$ be an input exemplar image, $\Omega = \{\Omega_e,\ 1 \le e \le N\} \subset \mathbb{R}^2$ be a discrete design domain under consideration made of disjoint square elements $\Omega_e$, as indicated in Fig. 1(b). A vector of discrete density $\boldsymbol{\rho} = \{\rho_e\}$ is defined over $\{\Omega_e\}$, where $\rho_e = 0$ or $\rho_e = 1$ indicates whether the element $\Omega_e$ is void or solid.

We aim to find an optimized 0–1 distribution of density $\boldsymbol{\rho}$, solid or void, at a certain volume reduction to meet both the criteria of physical optimality and visual similarity. The physical property is measured in terms of the body's stiffness, or reversely its compliance $C(\boldsymbol{\rho})$, representing its resistance to deformation. The geometric similarity, denoted as

$$\mathcal{S}_B(\boldsymbol{\rho}) = \|B - \mathcal{I}_B\|^r, \quad B \subset \Omega, \tag{1}$$

represents the minimal block-wise difference between a block $B \subset \Omega$ and one of the exemplar image $\mathcal{I}$ of the same size $\mathcal{I}_B$, whose concrete computation will be further detailed in Section 5.

Following the classical FE analysis, the problem of generative structural design is stated as follows: find the optimized density distribution vector $\boldsymbol{\rho} = \{\rho_e\} \in \mathbb{R}^N$ such that

$$(\mathcal{P}): \quad \min_{\boldsymbol{\rho}\in\mathbb{R}^N} C(\boldsymbol{\rho}) = \mathbf{u}^T\mathbf{K}(\boldsymbol{\rho})\mathbf{u}, \quad s.t. \tag{2}$$

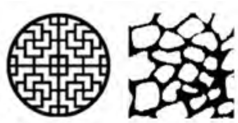

(a) Exemplar textures.

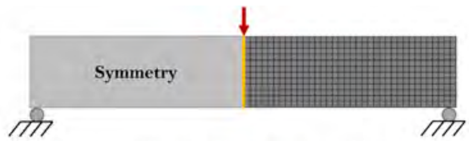


(b) A MBB example under volume fraction 0.5.

(c) Benchmark topology optimization result, $C = 202.1$.

(d) An optimized structure to the left texture in (a), $C = 259.3$.

(e) An optimized structure to the right texture in (a), $C = 224.4$.

**Fig. 1.** The problem of texture-guided generative structural design: given a certain design problem and exemplar textures, various structures, such as those in (d) and (e), are created using the proposed approach.

$$\begin{cases} \mathbf{K}(\boldsymbol{\rho})\mathbf{u} = \mathbf{f}(\boldsymbol{\rho}), \ \mathbf{u} \in \mathbb{R}^n, \\ V(\boldsymbol{\rho}) \le \nu V_0, \\ \mathcal{S}_B(\boldsymbol{\rho}) \le \delta_B, \ B \subset \Omega, \\ \rho_e = 0 \text{ or } 1, \ e = 1, \ldots, N. \end{cases}$$

Here, $\mathbf{u} \in \mathbb{R}^n$ is the vector of the nodal displacement to be computed, $\mathbf{K}(\boldsymbol{\rho})$ is the overall stiffness matrix, $\mathbf{f}(\boldsymbol{\rho})$ represents the nodal external loadings, $V(\boldsymbol{\rho})$ is the volume of the computed structure, and $\nu$ is the desired volume fraction, or specifically,

$$\mathbf{K}(\boldsymbol{\rho}) = \sum_{e=1}^{N} E_e(\rho_e)\mathbf{K}_e^0 \ \in \mathbb{R}^{nn}, \tag{3}$$

$$V(\boldsymbol{\rho}) = \sum_{e=1}^{N} \rho_e V_e, \quad V_e = \mathrm{Vol}(\Omega_e), \tag{4}$$

and

$$E_e(\rho_e) = E_{min} + \rho_e^p (E_0 - E_{min}), \tag{5}$$

where $\mathbf{K}_e^0$ is the unit per-element stiffness matrix, $E_0$ is the Young's modulus of the material, $E_{min}$ is a very small modulus assigned to void regions to avoid singular stiffness matrix, and $p$ is a penalty factor (typically $p = 3$) introduced to produce a near black-and-white solution.

Note here taking the input textures, the volume fraction $\nu$, and the similarity bound $\delta_B$ as design parameters will provide various optimized design options for generative design.

### 3.1. Discussions

Several other options may be chosen to formulate the problem, for example,

$$(\mathcal{P}_\lambda): \quad \arg\min_{\boldsymbol{\rho}} (\mathcal{S}_a(\boldsymbol{\rho}) + \lambda C(\boldsymbol{\rho})), \quad \text{for a constant } \lambda, \tag{6}$$

or

$$(\mathcal{P}_G): \quad \arg\min_{\boldsymbol{\rho}} (\mathcal{S}_a(\boldsymbol{\rho})), \quad s.t. \quad C(\boldsymbol{\rho}) \le C_{max}, \tag{7}$$

where $\mathcal{S}_a(\boldsymbol{\rho})$ is the global similarity measure set as the average of $\mathcal{S}_B(\boldsymbol{\rho})$, that is,

$$\mathcal{S}_a(\boldsymbol{\rho}) = \frac{\sum_{B\subset\Omega} \mathcal{S}_B(\boldsymbol{\rho})}{M}, \tag{8}$$

where $M$ is the number of blocks in the domain, $C_{max}$ has a default value of $1.2C_O$ for an optimized compliance $C_O$ derived from classical topology optimization approach.

Both of the above formulations use the *global* similarity (8), and formulation ($\mathcal{P}_G$) usually produces better results [9]. However, neither of the two formulations was chosen here due to following observations. Using the global measure (8), the optimizer has to distribute materials into some unimportant regions to maintain the overall geometric similarity. As a result, it unfortunately will deteriorate the structural rigidity or even produce a disconnected structure. Instead, the block-wise similarity $\mathcal{S}_B$ in $\mathcal{P}$ is able to finely tune the material contribution with respect to each block. Ultimately, it produces a mechanically more reliable structure, which is geometrically connected and smooth. Further details are to be shown in Section 4.

Alternatively, similar as previous studies [26], a soft-max p-norm was also able to reduce the number of constraints in problem $\mathcal{P}$. Specifically, it has the following form,

$$\max_{B\subset\Omega}(\mathcal{S}_B(\boldsymbol{\rho})) \approx \|\mathcal{S}_B(\boldsymbol{\rho})\|_p = (\sum_{B\subset\Omega} \mathcal{S}_B^p(\boldsymbol{\rho}))^{\frac{1}{p}}, \tag{9}$$

and the texture similarity constraint becomes

$$\mathcal{S}_B^N(\boldsymbol{\rho}) = \frac{(\sum_{B\subset\Omega} \mathcal{S}_B^p(\boldsymbol{\rho}))^{\frac{1}{p}}}{|\{B\}|} \le \delta_B. \tag{10}$$

However, as our experiment demonstrates, structures induced by the p-norm are more plausible to generate uneven tiny or big holes and to present bigger compliance. It is believed that the averaged similarity of the p-norm is lack of strict local enforcement. The comparisons between the numerical results is detailed in Section 6.1.

## 4. Optimization approach

### 4.1. Overall approach

Numerical approach to resolve the optimization problem $\mathcal{P}$ in (2) is first explained in this section. It involves two main steps: best-matching region detection, and density update. The region matching is based on previous study [8] while the density updating follows a gradient-based optimization and uses the well-established Globally Convergent Method of Moving Asymptotes (GCMMA) [32].

In addition, in order to further improve the approach's convergence and iteration speed, a multi-resolution scheme was also applied using a similar technique as that applied in [8]. It first starts from an optimization at a low resolution, and then up-scales to the next higher resolution using the lower resolution solution as an initial value. In particular, in order to improve the

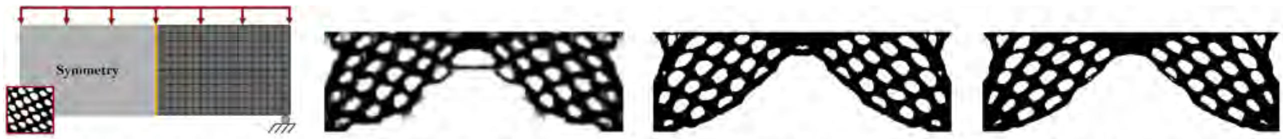


(a) A bridge example and exemplar texture. (b) Low resolution($50 \times 150$), $C = 10.0$. (c) Middle resolution($100 \times 300$), $C = 33.6$. (d) High resolution($200 \times 600$), $C = 132.9$.

**Fig. 2.** Framework of multi-resolution optimization.

structure connection of the final produced structure and its global smoothness, a physics-adaptive similarity regulator is designed. The overall optimization approach is briefly explained in Algorithm 1, followed by the algorithmic details.

**Algorithm 1** Texture-guided topology optimization.

**Input**: exemplar image $\mathcal{I}$, texture similarity bound $\delta_B$, target volume fraction $\nu$
**Output**: final deign field $\boldsymbol{\rho}$

**Initialize**: design field value $\boldsymbol{\rho} = \boldsymbol{\rho}_0$, block size $d = d_0$
**for** each resolution **do** // according to Section 4.2.
  **while** $\Delta\boldsymbol{\rho} > \epsilon$ **do**
    **Compute u** in problem $\mathcal{P}$ by FEM
    **Detect** the best matching $\mathcal{I}_B$ for each $B$
    **Compute** the texture energy $\mathcal{S}_B(\boldsymbol{\rho})$ for each $B$ and the volume $V(\boldsymbol{\rho})$
    **Compute** the sensitivities of the objective and constraints with respect to $\boldsymbol{\rho}$ using approaches in Section 4.3
    **Do** global similarity regulations and histogram matching using approaches in Section 5
    **Update** $\boldsymbol{\rho}$ via GCMMA using the above computed objective and constraints, and their associated sensitivities
  **Update** up-scale $\boldsymbol{\rho}$, $d = 2d$

*4.2. Multi-resolution optimization*

A multi-resolution optimization procedure was applied to avoid undesirable local minimum and to improve the convergence speed, as also observed by Kwatra et al. [8]. A three-resolution optimization procedure is applied in this study. It first starts from an optimization at a low resolution by using design domain $\Omega$, whose size is set as a quarter of size of the target domain. Meanwhile, the associated block size for $B \in \Omega$ is also set as a quarter of the prescribed one of default value 80. The derived optimized solution to this low resolution problem was then up-scaled to the next higher resolution as an initial value to find the next optimized solution. The up-scaled procedure was achieved using a bilinear interpolation scheme, both for the design domain $\Omega$ and the block $B$. The framework of multi-resolution optimization about a bridge example is shown in Fig. 2.

*4.3. Sensitivity analysis and filters*

Even with the relaxations from the discrete optimization to a continuous optimization problem, the topology optimization $\mathcal{P}$ in (2) is still very challenging due to the inclusion of the nonlinear similarity constraint, which results in an overall complex nonlinear and nonconvex optimization problem. The classical optimal criteria (OC) approach is not applicable to resolve this issue because of the additional similarity constraint. Due to these considerations, the well-established optimization approach GCMMA was applied here [32]. It approximates the original nonconvex problem through a set of convex subproblems by using the gradients of the optimization objective and constraints with respect to the design density. Details are explained below.

The approach depends on computation of the derivatives of the objective function $C(\boldsymbol{\rho})$ and constraints $\mathcal{S}_B(\boldsymbol{\rho})$, as defined in $\mathcal{P}$ in (2), with respect to the density $\rho_e$. They are derived as follows:

$$\frac{\partial C(\boldsymbol{\rho})}{\partial \rho_e} = -p\rho_e^{p-1}(E_0 - E_{min})\mathbf{u}_e^T\mathbf{K}_e^0\mathbf{u}_e, \tag{11}$$

$$\frac{\partial V(\boldsymbol{\rho})}{\partial \rho_e} = V_e/N, \tag{12}$$

$$\frac{\partial \mathcal{S}_B(\boldsymbol{\rho})}{\partial \rho_e} = \frac{2w_B(B - \mathcal{I}_B)}{\delta_B}, \tag{13}$$

where $N$ is the number of discrete elements $\Omega_e$. The derivative of similarity constraint in Eq. (13) is based on the similarity expression later given in Eq. (19).

The direct use of the above-derived sensitivities usually produces undesired structures of checkerboard patterns and large regions of gray scale. To avoid this issue and to ensure solution existence, the above-computed sensitivities were further filtered by the following approach.

Let

$$\widetilde{\rho}_e = \frac{1}{\sum_{i \in D_e} H_{ei}} \sum_{i \in D_e} H_{ei}\rho_i, \tag{14}$$

where $D_e$ is the set of elements $\Omega_i$ with distance to $\Omega_e$ smaller than a given radius $r_{min}$, and

$$H_{ei} = max(0, r_{min} - \|\Omega_i - \Omega_e\|). \tag{15}$$

Then the sensitivity can be computed following the chain rule

$$\frac{\partial \psi}{\partial \rho_e} = \frac{\partial \psi}{\partial \widetilde{\rho}_e}\frac{\partial \widetilde{\rho}_e}{\partial \rho_e} = \frac{\partial \psi}{\partial \widetilde{\rho}_e} \cdot \frac{1}{\sum_{i \in D_e} H_{ei}} H_{ei}, \tag{16}$$

where function $\psi$ can be the objective function $C(\boldsymbol{\rho})$ or constraints $\mathcal{S}_B(\boldsymbol{\rho})$ and $V(\boldsymbol{\rho})$.

In addition, the smooth filter proposed by Wu et al. [26] was also implemented in the approach to ensure a black-and-white solution and for convergence improvement.

## 5. Similarity and regulation

Details on defining the similarity measure $\mathcal{S}_B(\boldsymbol{\rho})$ involved in problem (2) are explained in this section. In particular, the physics-adaptive regulator is defined and its usages are explained.

*5.1. Similarity measure*

Given a structure $\boldsymbol{\rho}$ and an input texture exemplar image $\mathcal{I}$, their similarity can be defined by any type of energy whose first derivatives are available. A sufficient condition for a structure $\boldsymbol{\rho}$ being similar to an exemplar image $\mathcal{I}$ is that all blocks $B$ of certain prescribed size in the structure are similar to some blocks in exemplar $\mathcal{I}$. See Fig. 3 for an illustration.

Inspired by this, a local block-wise texture energy, or *block-wise similarity*, is proposed for fine-tuned local feature control, following a global energy defined in [8]. Specifically, given a discrete

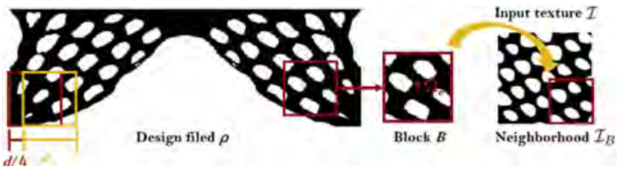


**Fig. 3.** Illustration of the definition of block-wise similarity $\mathcal{S}_B(\boldsymbol{\rho})$ between a design density $\boldsymbol{\rho}$ and an input texture exemplar $\mathcal{I}$ for a specific block $B$.

mesh element $\Omega_e$, we defined its associated block $B(\Omega_e)$, $B$ for short, as the set of discrete elements $\Omega_j$ surrounding $\Omega_e$, that is,

$$B(\Omega_e) = \{\Omega_j \mid \|\Omega_j - \Omega_e\| < d/2,\ \Omega_j \in \Omega\}. \tag{17}$$

Let $\mathcal{I}_B \subset \mathcal{I}$ be a neighborhood of size $d$ in $\mathcal{I}$ that is the most similar to $B$ in terms of the p-norm in Euclidian space. We defined the texture similarity energy of $B$ with respect to $\mathcal{I}_B$ as norm of their point-wise density difference, that is,

$$\mathcal{S}_B(\boldsymbol{\rho}) = \|B - \mathcal{I}_B\|^r = (\sum_{e\in B}(B_e - \mathcal{I}_e)^r)^{\frac{1}{r}}. \tag{18}$$

In practical computation of $\mathcal{S}_B(\boldsymbol{\rho})$, we build a KD-tree of textures and find the best matching neighborhood $\mathcal{I}_B$ for every $B \subset \Omega$, based on a previous approach in [6,7]. It has an average time complexity of searching of $O(logM)$, for the block number $M$ in the domain. Using KD-tree to find nearest neighborhood can efficiently eliminate the large portions of the search space.

In addition, it is desirable not to considerably change block $B$ if it is already close to $\mathcal{I}_B$. Therefore, we set exponent $r = 1.2$, which allows the optimization to be more robust against outliers, following a strategy similar to that used in [8]. Alternatively, we apply iteratively re-weighted least squares (IRLS) [33] on similarity measure $\mathcal{S}_B(\boldsymbol{\rho})$ and Eq. (18) becomes

$$\mathcal{S}_B(\boldsymbol{\rho}) = \|B_0 - \mathcal{I}_B^0\|^{r-2}\|B - \mathcal{I}_B\|^2 = w_B\|B - \mathcal{I}_B\|^2, \tag{19}$$

where weights $w_B$ are taken as constants in each iteration step and evaluated using the value of $B_0$ and $\mathcal{I}_B^0$ in the last iteration. Note also $\mathcal{I}_B$ is the parameter to be determined in the optimization process.

In practice, in computing the solution to problem $\mathcal{P}$, only a subset of $\{\Omega_e\}$ is considered to reduce the computation efforts. The subsets are supposed to sufficiently overlap with each other, and are empirically chosen to comprise block centers $d/4$ apart, as indicated in Fig. 3; similar strategy was also used in [8]. This choice prevents the final generated structures from becoming extremely blurry in regions between overlapping blocks.

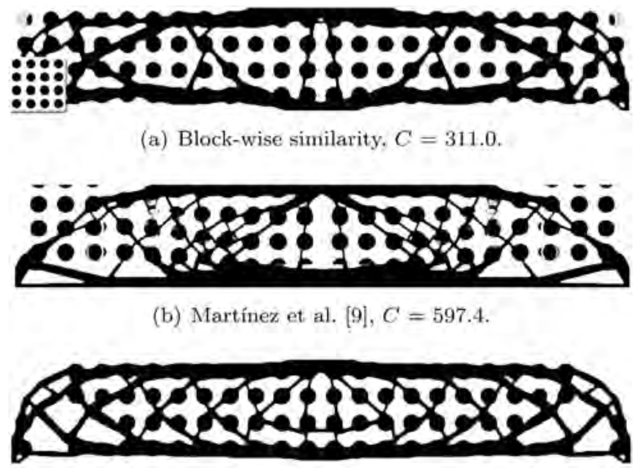

(a) Block-wise similarity, $C = 311.0$.

(b) Martínez et al. [9], $C = 597.4$.

(c) Geometry-adaptive similarity, $C = 257.3$.

**Fig. 5.** Comparisons between structures generated based on block-wise similarity and geometry-adaptive similarity for the MBB example in Fig. 1. The exemplar is on the bottom left in (a).

### 5.2. Similarity regulation

Directly utilizing the block-wise similarity measure (19) in the optimization problem $\mathcal{P}$ still has difficulty in balancing the compliance minimization and geometric similarity, and may produce disconnected regions; see for example in Fig. 5(a). And the undesirable protrusions are to be improved via a novel *physics-adaptive* similarity regulator as detailed below.

*Block-wise geometry-adaptive regulation.* First consider the example in Fig. 5(b) as a failed example first shown in [9]. In order to resolve issue, the priority of each block in contributing to the final design is further included in Eq. (19), where the similarity requirement is less enforced for nearly void region. We consequently have the regulated *geometry-adaptive similarity* measured as follows,

$$\mathcal{S}_B^G(\boldsymbol{\rho}) = b_B w_B\|B - \mathcal{I}_B\|^2, \tag{20}$$

where $b_B$ is a weighted positive real value to indicate the contribution of each block, that is,

$$b_B = (\sum_{e\in B}\boldsymbol{\rho}_e)/|B|, \tag{21}$$

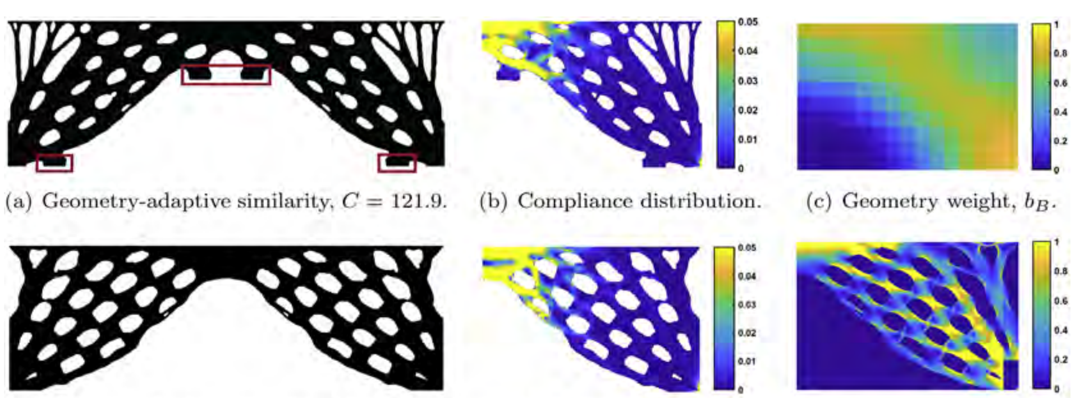


(a) Geometry-adaptive similarity, $C = 121.9$. (b) Compliance distribution. (c) Geometry weight, $b_B$.

(d) Physics-adaptive similarity, $C = 132.9$ (e) Compliance distribution. (f) Physics weight, $b_B c_e$.

**Fig. 4.** Different similarity measurements produce very different optimized structures. The block-wise geometry-adaptive similarity may produce structures exhibiting protrusion outlined in red in (a). The physics-adaptive similarity produces a mechanically sound and geometrically smooth optimized structure . (For interpretation of the references to color in this figure legend, the reader is referred to the web version of this article.)

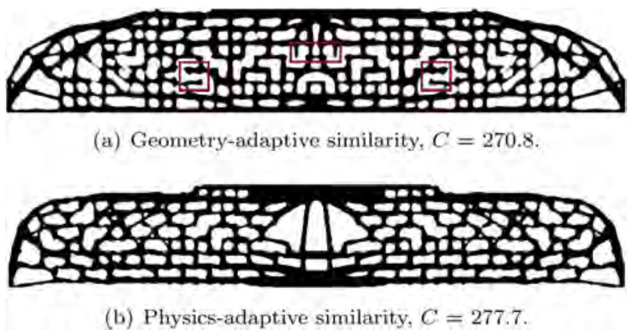

(a) Geometry-adaptive similarity, $C = 270.8$.

(b) Physics-adaptive similarity, $C = 277.7$.

**Fig. 6.** Given a complex and sharp texture in Fig. 1(a) and certain design problem in Fig. 1(b), the structure generated by geometry-adaptive regulation has many undesirable protrusions in red boxes in (a). But physics-adaptive regulation still produces smooth structure . (For interpretation of the references to color in this figure legend, the reader is referred to the web version of this article.)

where $|B|$ stands for the number of elements in block $B$. The regulation is block-wise and the similarity measure $\mathcal{S}_B^G(\boldsymbol{\rho})$ is computed per-element.

Using the novel geometry-adaptive regulated similarity, a region connected and mechanically stable structure is created as shown in Fig. 5(c). Its structural compliance is also smaller than those derived by the other two approaches (Fig. 5(a) and (b)). Note that the work of Martinez et al. [9], as similarly defined in $P_G$, does not seek to minimize the compliance explicitly, but only constrains it to stay below a given threshold.

*Physics-adaptive regulation.* The above geometry-adaptive similarity in Eq. (20) helps resolve the structural connection issue but may still produce unsmooth structures. See for example the undesirable protrusions in red boxes in the optimized structure in Fig. 4(a).

Taking a close observation of the per-element compliance distribution in Fig. 4(b) — the undesirable local regions have very small compliance. In addition, we also notice that the geometric smoothness is essentially a natural consequence from mechanical soundness, as can also be observed from the various structures derived via classical topology optimization approaches. Based on the observations, we can thus design a *physics-adaptive* regulator to further adjust the similarity measure in Eqs. (20), which takes the following form,

$$\mathcal{S}_B^P(\boldsymbol{\rho}) = b_B w_B \sum_{e\in B} \|c_e(B_e - \mathcal{I}_B^e)\|^2, \tag{22}$$

where $c_e$ is the compliance of each element $\Omega_e$ in block $B$. Using the novel similarity ultimately produces the structure in Fig. 4(d) of smooth boundary.

Smooth boundary is guaranteed and it does not rely on the interior smoothness of the texture. Even for complex and sharp texture in Fig. 1(a), physics-adaptive regulation still work, as shown in Fig. 6.

### 5.3. Histogram matching

Direct application of the above-mentioned approaches may produce some blurry blending or aberrant elements. We further resolve this issue by adopting position and index histogram matching of global statistics, first proposed by Kopf [28]. Kopf also discovered that the histogram matching could avoid local minimum and match exemplar better, meanwhile dramatically improving the convergence of the iteration.

Technically, let $H_\rho$ and $H_\mathcal{I}$ be the histograms of $\boldsymbol{\rho}$ associated to domain $\Omega$ and the input exemplar image $\mathcal{I}$. We define a modified weight $\tilde{w}_B$ involved in (19)

$$\tilde{w}_B = \frac{w_B}{1 + max(0, H_\rho(\mathcal{I}_B) - H_\mathcal{I}(\mathcal{I}_B))}, \tag{23}$$

where, $H_\rho(\mathcal{I}_B)$ stands for the number of $\mathcal{I}_B$ being chosen as best matching neighborhoods for all sample blocks in the density field $\boldsymbol{\rho}$, $H_\mathcal{I}(\mathcal{I}_B)$ counts the number of neighborhoods in $\mathcal{I}$ geometrically similar to $\mathcal{I}_B$. The corresponding regulated similarity is then defined

$$\mathcal{S}_B^G(\boldsymbol{\rho}) = b_B \tilde{w}_B \|B - \mathcal{I}_B\|^2, \tag{24}$$

or

$$\mathcal{S}_B^P(\boldsymbol{\rho}) = b_B \tilde{w}_B \sum_{e\in B} \|c_e(B_e - \mathcal{I}_B^e)\|^2 \tag{25}$$

## 6. Experiments

The proposed approach was implemented in MATLAB on a computer with an Intel Core i7, 3.7 GHz CPU and 32 GB RAM. All the design domains are assumed comprising of materials of Poisson's ratio $\nu = 0.3$, Young's modulus $E_0 = 1$ and $E_{min} = 1e - 9$. A three-resolution optimization process was adopted. In the first resolution, the block size is $d = 20$, and the design domain size is a quarter of the size of the target domain. The design domain in the second resolution is half the size of the target domain. In addition, the iteration step is set 100 in the low resolution, 150 in the middle resolution, and 50 in the high resolution. Experiments show that the settings generally result in a convergent solution. The associated computation time is also summarized in Table 2.

All the examples use the physics-adaptive regulator (22) except the one in Fig. 12 using geometry-adaptive regulator in (20). We set by default the similarity bound $\delta_{low} = 3.5$ in the low resolution, $\delta_{middle} = \delta_{low} + 0.3$ and $\delta_{high} = \delta_{middle} + 0.3$, as involved in (2).

The smoothness of the derived structures is quantitatively measured using the number edges of its outer boundary, extracted using Sobel operator detection method [34,35]. The smaller the value, or less number of outer boundary edges, the more smooth the structure.

### 6.1. Overall performance and comparisons

The overall performance of the proposed approach was first explained using the example in Fig. 7, including its comparisons with various other possible similarity measures, and its convergence performance.

*Comparison.* We first compare the optimized structure obtained via benchmark topology optimization, direct texture synthesis, Martínez et al. [9], soft max p-norm similarity, geometry-adaptive similarity, and the proposed physics-adaptive similarity, respectively shown in Fig. 7(a–f). Table 1 also compares the concrete values of the derived structures' compliance, smoothness, running time using these different approaches.

As can be seen from the results, the structure produced by geometry-adaptive regulator has the best compliance amongst them, while simply texture synthesis produces the worst. Notice that the structure produced via physics-adaptive regulator is very smooth in its boundary while either the one produced by the geometry-adaptive one or by Martínez et al. [9] has unwanted protrusion. We also observe that the running time of the proposed approach is higher than that of [9]. This is understandable as including more design constraints usually results in a more complex optimization problem. P-norm similarity spends the least time by reducing the number of similarity constraints. However, the averaged similarity is more possible to generate uneven tiny or big holes.

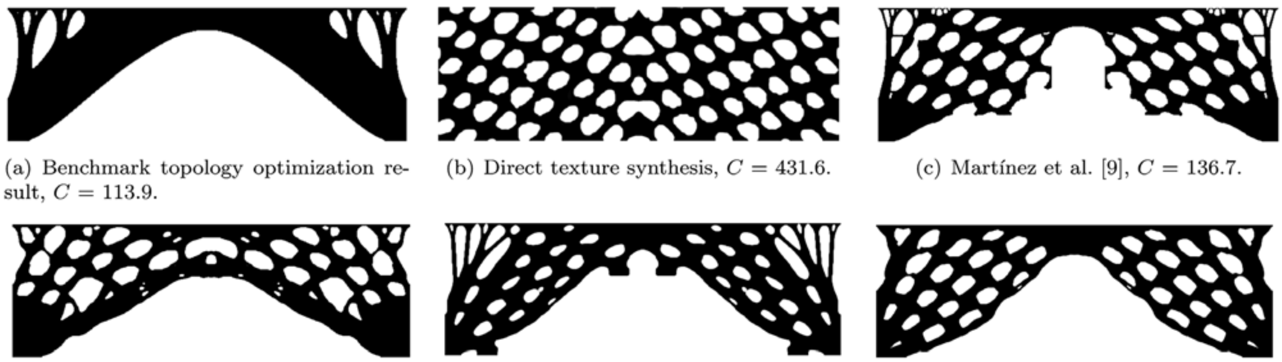

(a) Benchmark topology optimization result, $C = 113.9$.
(b) Direct texture synthesis, $C = 431.6$.
(c) Martínez et al. [9], $C = 136.7$.
(d) P-norm in (10), $C = 139.7$.
(e) Geometry-adaptive similarity, $C = 121.9$.
(f) Physics-adaptive similarity, $C = 132.9$.

**Fig. 7.** Given an exemplar texture and certain design problem in (a), the structures generated by various optimization approaches are produced. In particular, (f) overcome the difficulties of region disconnections in [9] and removes the protrusions in (c) and (e).

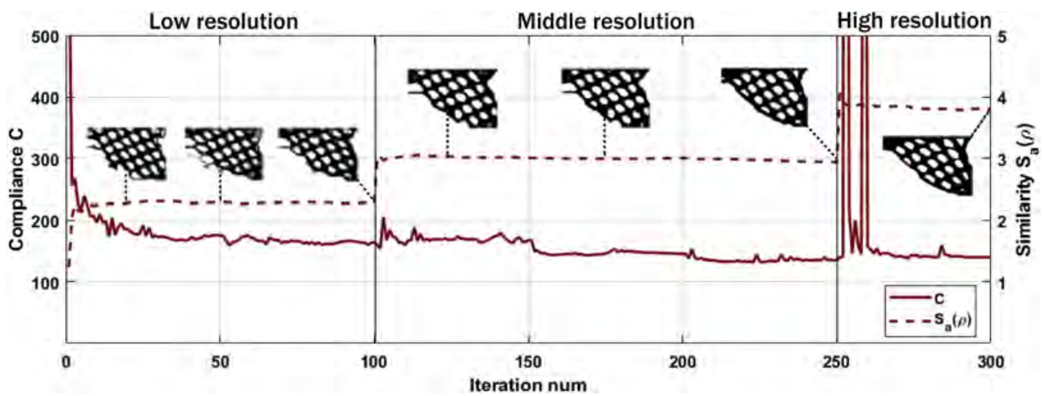


**Fig. 8.** Convergence curves of the proposed optimization approach on the variations of the scaled structural compliance and associated average similarity energy defined in (8).

**Table 1**
Comparison and measurements of different regulation strategies.

| Regulation | Model | Physical performance $C$ | Geometry similarity $\mathcal{S}_a(\boldsymbol{\rho})$ | Smoothness | Total time |
|---|---|---|---|---|---|
| Martínez | Fig. 7(c) | 136.7 | 3.4 | 543 | 3.3 |
| P-norm | Fig. 7(d) | 139.7 | 3.4 | 372 | 2.4 |
| Geometry- | Fig. 7(e) | 121.9 | 4.0 | 403 | 10.0 |
| Physics- | Fig. 7(f) | 132.9 | 3.7 | 367 | 10.0 |

**Table 2**
Summary of time costs for the numerical examples.

| Figure | Model | Domain size | Exemplar size | Simulation time | Matching time | Total time |
|---|---|---|---|---|---|---|
| Fig. 7 | Bridge | $200 \times 600$ | $200 \times 200$ | 0.9 | 0.4 | 10.0 |
| Fig. 9 | MBB | $120 \times 720$ | $200 \times 200$ | 0.6 | 0.2 | 4.1 |
| Fig. 15 | Interior | $200 \times 200$ | $150 \times 150$ | 0.8 | 0.1 | 2.8 |
| Fig. 16 | L-Beam | $200 \times 200$ | $100 \times 100$ | 0.6 | 0.1 | 13.7 |
| Fig. 17 | Tower | $100 \times 600$ | $150 \times 150$ | 0.9 | 0.1 | 10.8 |

*Times measured in minutes.

*Convergence.* We further explore during the iteration process the variations of the structural compliance and the averaged similarity energy in (8), and depicted it in Fig. 8. Since the size of design domain has changed during the multi-resolution optimization process, we scaled accordingly the base element's stiffness matrix for consistent comparison across different resolutions.

We can observe from the results, abrupt compliance jumps happen in the highest resolution, but it does not change the overall convergence of the whole optimization approach. In addition, the similarity curve (about average similarity energy $\mathcal{S}_a(\boldsymbol{\rho})$ in (8)) remains flat during the whole iteration steps. This interesting phenomenon indicates that the similarity requirement is generally satisfied during the optimization process.

### 6.2. Effect of optimization parameters

We further test for problem (2) in this section the effect of the design parameters, specifically similarity bounds $\delta_B$, volume fractions $\nu$ and input exemplars, in generating different

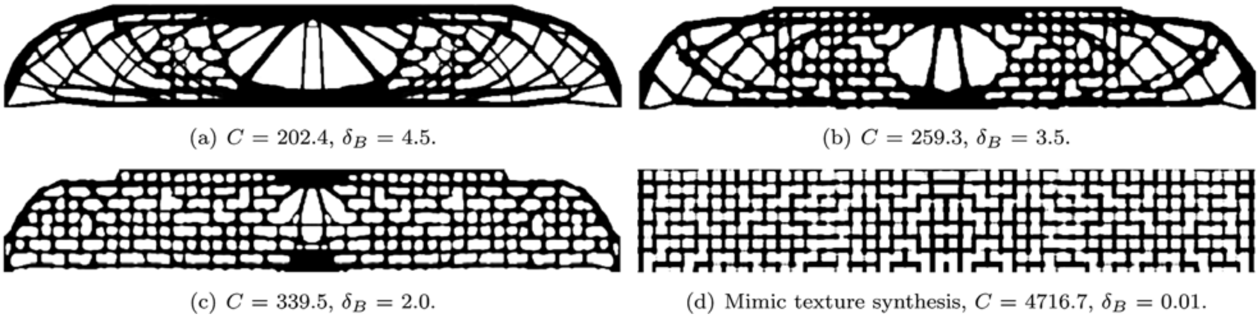

(a) $C = 202.4$, $\delta_B = 4.5$. (b) $C = 259.3$, $\delta_B = 3.5$. (c) $C = 339.5$, $\delta_B = 2.0$. (d) Mimic texture synthesis, $C = 4716.7$, $\delta_B = 0.01$.

**Fig. 9.** Numerical results on different similarity requirements for the MBB example in Fig. 1. The volume fractions $\upsilon = 0.5$.

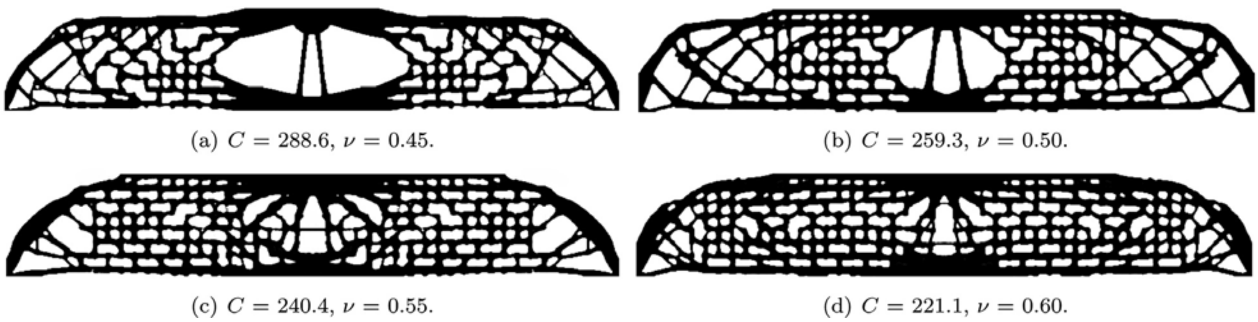

(a) $C = 288.6$, $\nu = 0.45$. (b) $C = 259.3$, $\nu = 0.50$. (c) $C = 240.4$, $\nu = 0.55$. (d) $C = 221.1$, $\nu = 0.60$.

**Fig. 10.** Numerical results on different volume fractions for the MBB example in Fig. 1. The similarity bounds $\delta_B = 3.5$.

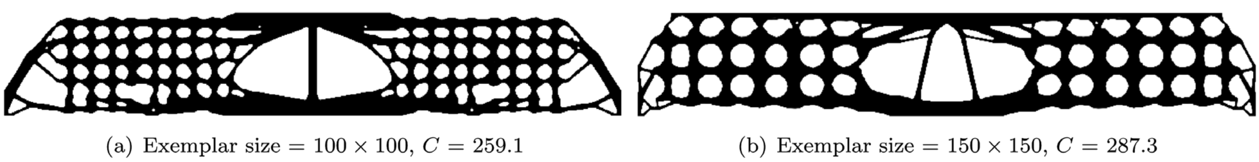

(a) Exemplar size = $100 \times 100$, $C = 259.1$ (b) Exemplar size = $150 \times 150$, $C = 287.3$

**Fig. 11.** Numerical results on hole size control for the MBB example in Fig. 1. The volume fractions $\upsilon = 0.5$, and the texture similarity bounds $\delta_B = 3.0$.

optimized structures. The MBB example in Fig. 1 is used for this test.

*Different similarity bounds $\delta_B$.* In this test, the similarity bounds $\delta_B$ are respectively set 4.5, 3.5, 2.0 and 0.01, and their associated optimized structures are shown in Fig. 9(a–d). The benchmark structure produced via classical topology optimization approach is also shown in Fig. 1(c) for comparison. We can see from the results that $\delta_B$ nicely balances the geometric similarity and structural compliance. As $\delta_B$ decreasing from (a) to (d), the similarity requirements are enforced more strictly, producing structures of better appearance approximations but of large compliance or equivalently worse physical performance. These different structures may apply to different design purposes.

*Different volume fractions $\nu$.* In this test, we keep the similarity bound $\delta_B = 3.5$ unchanged and the volume fractions $\nu$ are respectively set 0.45, 0.50, 0.55, 0.60. The produced structures are respectively shown in Fig. 10(a–d). As can be seen from the results, as the material volume $\nu$ increases, more solid regions start to appear in the optimized structures of smaller associated compliance.

*Different block sizes b.* The block size $b$ is up-scaled to the next resolution in our approach, as described in Section 4.2. This is different from previous approaches that used fixing block size across different resolutions so that blocks at the low resolution cover more spatial extent. In order to explore their difference, we also show the result in Fig. 13 at fixing block size $b = 20$; see its comparison of up-scaled size in Fig. 9(b). Some undesired protrusions are also observed in the results in Fig. 13. Their respective constraint numbers are 1450 and 46, taking time 135.9 mins and 4.1 mins to obtain the result. As we can see, the case of fixing block size dramatically increases the number of constraints, which leads to larger computational time.

*Effect on hole sizes.* Adjusting the sizes of an input exemplar image via up-scaling the input exemplar, as shown in Fig. 14, is also able to control the hole sizes of the optimized structures for different design purposes (see Fig. 11). In this example, the target volume fraction $\nu$ is 0.5, and the similarity bound $\delta_B$ is 3.0. As can be seen from the results, the holes in the produced structures becomes larger as the input exemplar size increases. In addition, the overall porous structures maintain their similarity with the different sized input textural exemplars, demonstrating the effect of the proposed approach.

*Effect on structural thickness.* The proposed approach's ability in controlling structure thickness is tested and shown in Fig. 12. In this example, the similarity bounds $\delta_B = 2.1$, the target volume fractions are respectively 0.5 and 0.6. This time, we particularly choose the geometry-adaptive regulator for better geometric similarity. The produced structures demonstrate their close geometric similarity to the input exemplar images in all the cases, while simultaneously exhibiting close compliance to the benchmark result produced by classical topology optimization.

### 6.3. Different design problems

*Effect of interior design at distributed forces.* The square examples at distributed forces in Fig. 15 are tested. The volume fractions are

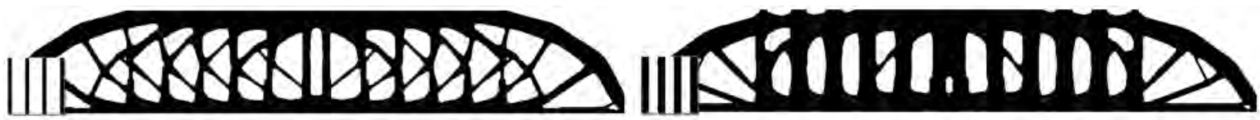

(a) $C = 208.8$, $v = 0.5$. (b) $C = 198.2$, $v = 0.6$.

**Fig. 12.** Numerical results on thickness control on the MBB example in Fig. 1. The exemplars size is104 × 99, and the texture similarity bounds $\delta_B = 2.1$.

**Fig. 13.** Numerical results on fixing the block size across different resolutions ($C$ = 428.0, times = 135.9 mins).

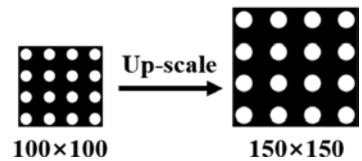


**Fig. 14.** Generating exemplars of different sizes via up-scaling, from sizes 100 × 100 to 150 × 150.

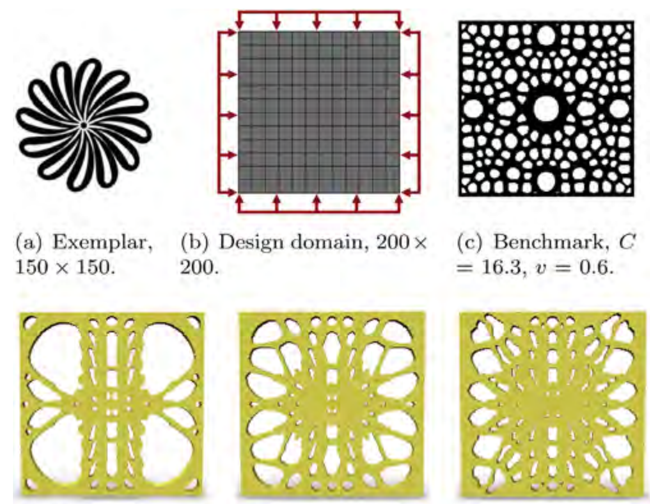

(a) Exemplar, 150 × 150. (b) Design domain, 200 × 200. (c) Benchmark, $C$ = 16.3, $v = 0.6$.

(d) $C = 28.9$, $v = 0.5$. (e) $C = 20.3$, $v = 0.6$. (f) $C = 15.8$, $v = 0.7$.

**Fig. 15.** Numerical results on constraints of different volume fractions for an interior design at distributed forces. The texture similarity bounds $\delta_B = 3.0$.

(a) Design domain, 200 × 200. (b) Benchmark, $C$ = 195.6. (c) $C = 229.5$.

**Fig. 16.** Numerical results on classical L-Beam. The texture similarity bound $\delta_B$ = 3.0 and the volume fraction $v = 0.5$.

set 0.5, 0.6 and 0.7, and the associated structures are respectively shown in Fig. 15(d–f). The complex boundary conditions raise further optimization challenges, and expected examples were also produced for the various design cases.

*Effect of L-Beam example.* We also test the approach's performance on the classical L-Beam in Fig. 16, which does not have left–right symmetry. In this example, the block size $d$ is maintained the same in the middle resolution to achieve more delicate texture control, and it is scaled three times in the highest resolution to reduce the constraint number. Its comparison with the classical topology optimization result in Fig. 16(b) shows that the proposed approach also works well in such case.

*Effect of tower example.* The more complex example of a simplified Eiffel Tower is also conducted to further test the approach's performance. The problem was constructed based on the study of the Johns Hopkins University[3] and Warshawsky [36]. In this example, the two solid areas inside the tower are designed to imitate the platforms for man riding. Three types of loads act on the Eiffel Tower: its own weight, the weight of people and machinery on the platforms and wind load. The tower-weight is indicated by the two red arrows, and the bottom is twice as that of the top to indicate their gravity weight relation. The wind load is equivalent to an idealized point load acted at the top and halfway up the tower, and indicated by the blue arrow.

The produced structures are shown in Fig. 17, compared with the benchmark topology optimization result. As we can see, apart from well-balanced appearance similarity, all the derived structures showed close structure compliances to that of the benchmark topology optimization result. We particularly notice that the compliance of generated structure in Fig. 17(c) even demonstrates a smaller compliance (better structure) than that of the benchmark.

### 6.4. Generative design

Using different input textures and controlling parameters $\nu$, $\delta_B$ is able to produce huge amount of optimized structures for generative design. One of the results is shown in Fig. 18 for the Bridge example in Fig. 7. For every group of structures, the input texture is shown on the bottom left, and the corresponding structural compliance and design parameters are also shown below each figure. These generated various structures provide a large range of design candidates for the designer.

As can be observed from the results, the approach is able to adapt to various kinds of textures, subject to certain similarity requirement $\delta_B$ and volume constraint $\nu$ prescribed in (2). Generally the smaller value of the similarity requirement $\delta_B$, the worse structure produced with larger compliance. In addition, a larger value of volume constraint $\nu$ allows more material usage, and thus usually produces better structure of smaller compliance. The results indicate such consistency in general. We also notice that it is however not always the case due to the unavoidable local optimality of topology optimization problem; see for example the results in the second or last row in Fig. 18 for the cases $\delta_B = 3.5$ and 4.0.

[3] Perspectives on the Evolution of Structures, http://www.ce.jhu.edu/perspectives/studies/Eiffel/%20Tower/%20Files/ET_Loads.htm.

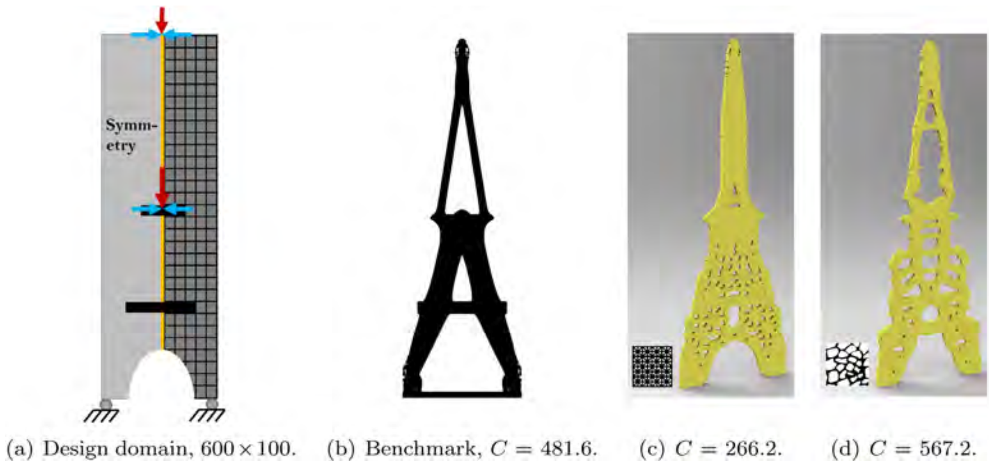


**Fig. 17.** Numerical results for simple simulation of the Eiffel Tower. The volume fractions $\upsilon = 0.45$, the texture similarity bounds $\delta_B = 5$, and the texture exemplar size is $150 \times 150$.


**Fig. 18.** Gallery of the generative designs created using different input textures, similarity bounds $\delta_B$, or volume fractions $\nu$.

## 7. Conclusion

The paper proposes a novel approach for generative design via producing various mechanical optimized structures guided by input image exemplars. The problem was formulated as a compliance minimization problem under a set of block-wise texture-similarity constraints. Owing to its novel problem formulation and physics-adaptive regulator, the approach is able to produce various geometrically and physically reasonable structures, as demonstrated by various numerical examples.

The proposed approach still have much room for improvement particularly on the following aspects. Firstly, further taking into account of texture orientation in the optimization design may help to align the texture features with the stress distributions to further improve its physical property. The recent excellent study conducted by Liu and Shapiro [30] has demonstrated the usage of texture orientations and may help to resolve the issue.

Next, the present approach has demonstrated its performance in various feature controls such as hole size or thickness control, and produces a structure globally similar to the input texture image. However, it is not able to accurately control the geometric features of the structure, for example, requiring its overall thickness strictly within certain range; see also the results in Fig. 15. Developing more advanced similarity measures or different controlling techniques may be able to help resolve the issue.

Finally, the present approach is mainly developed for generating various 2D structures. Its extension to generating 3D structures using a single 2D exemplar image will further explore its practical industrial applications, and is also much more demanding. It involves a topics on generating 3D structures from 2D images [28], and associated topology optimization approach, not to mention the much high computational complexity. The topic is under our present study.

## Acknowledgments

The work described in this paper is partially supported by the NSF of China (No. 61472356), and the National Key Research and Development Program (2016YFC1101302) from the MIST of China.

## References

[1] Bentley P. Evolutionary Design by Computers. San Francisco, Calif: Morgan Kaufmann Publishers; 1999.
[2] DreamCatcher, https://www.autodesk.com/solutions/generative-design.
[3] Rozvany GIN. A critical review of established methods of structural topology optimization. Struct Multidiscip Optim 2009;37:217–37.
[4] Sigmund O, Maute K. Topology optimization approaches: a comparative review. Struct Multidiscip Optim 2013;48(6):1031–55.
[5] Fratzl P, Weinkamer R. Nature's hierarchical materials. Progress in Materials Scienc 2007;52(8):1263–334.
[6] Efros AA, Leung TK. Texture synthesis by non-parametric sampling. In: Proceedings of the Seventh IEEE International Conference on Computer Vision(ICCV), 02. Washington, DC, USA: IEEE Computer Society; 1999, p. 1033–8.
[7] Wei L-Y, Levoy M. Fast texture synthesis using tree-structured vector quantization. In: Proceedings of the 27th Annual Conference on Computer Graphics and Interactive Techniques. New York, NY, USA: ACM Press/Addison-Wesley Publishing Co.; 2000, p. 479–88.
[8] Kwatra V, Essa I, Bobick A, Kwatra N. Texture optimization for example-based synthesis. ACM Trans. Graph. 2005;24(3):795–802.
[9] Martínez J, Dumas J, Lefebvre S, Wei L-Y. Structure and appearance optimization for controllable shape design. ACM Trans. Graph. 2015;34 (6):229:1–229:11.
[10] Bendsøe MP, Kikuchi N. Generating optimal topologies in structural design using a homogenization method. Comput Methods Appl Mech Engrg 1988;71(2):197–224.
[11] Bendsøe MP. Optimal shape design as a material distribution problem. Struct Optim 1989;1(4):193–202.
[12] Mattheck C, Burkhardt S. A new method of structural shape optimization based on biological growth. International Journal of Fatigu 1990;12 (3):185–90.
[13] Young V, Querin OM, Steven GP, Xie YM. 3D and multiple load case bi-directional evolutionary structural optimization (BESO). Struct Multidiscip Optim 1999;18(2):183–92.
[14] Allaire G, Jouve F, Toader AM. A level-set method for shape optimization. Comptes Rendus Mathematiqu 2002;334(12):1125–30.
[15] Wang MY, Wang X, Guo D. A level set method for structural topology optimization. Comput Methods Appl Mech Engrg 2003;192(1–2):227–46.
[16] Qian X. Topology optimization in B-spline space. Comput Methods Appl Mech Engrg 2013;265:15–35.
[17] Sigmund O. On the design of compliant mechanisms using topology optimization. Mech Struct Mach 1997;25(4):493–524.
[18] Haber RB, Jog CS, Bendsøe MP. A new approach to variable-topology shape design using a constraint on perimeter. Structural optimization 1996;11 (1):1–12.
[19] Cheng G, Mei Y, Wang X. A feature-based structural topology optimization method. In: M. P. Bendsøe O Sigmund, editor. IUTAM Symposium on Topological Design Optimization of Structures, Machines and Materials. Dordrecht: Springer Netherlands; 2006, p. 505–14.
[20] Chen S, Wang MY, Liu AQ. Shape feature control in structural topology optimization. Comput Aided Des 2008;40(9):951–62.
[21] Guo X, Zhang W, Zhong W. Explicit feature control in structural topology optimization via level set method. Comput Methods Appl Mech Engrg 2014;272:354–78.
[22] Langelaar M. An additive manufacturing filter for topology optimization of print-ready designs. Struct Multidiscip Optim 2017;55(3):871–83.
[23] Qian X. Undercut and overhang angle control in topology optimization: A density gradient based integral approach. Internat J Numer Methods Engrg 2017;111(3):247–72.
[24] Guo X, Zhou J, Zhang W, Du Z, Liu C, Liu Y. Self-supporting structure design in additive manufacturing through explicit topology optimization. Comput Methods Appl Mech Engrg 2017;323:27–63.
[25] Wu J, Wang CC, Zhang X, Westermann R. Self-supporting rhombic infill structures for additive manufacturing. Comput Aided Des 2016;80:32–42.
[26] Wu J, Aage N, Westermann R, Sigmund O. Infill optimization for additive manufacturing-approaching bone-like porous structures. IEEE transactions on visualization and computer graphics 2018;24(2):1127–40.
[27] Wei L-Y, Lefebvre S, Kwatra V, Turk G. State of the Art in Example-based Texture Synthesis. In: Eurographics 2009, State of the Art Report, EG-STAR. Munich, Germany: Eurographics Association; 2009, p. 93–117.
[28] Kopf J, Fu C-W, Cohen-Or D, Deussen O, Lischinski D, Wong T-T. Solid texture synthesis from 2D exemplars. ACM Trans. Graph. 26 (3).
[29] Liu X, Shapiro V. Random heterogeneous materials via texture synthesis. Computational Materials Scienc 2015;99:177–89.
[30] Liu X, Shapiro V. Sample-based synthesis of two-scale structures with anisotropy. Comput Aided Des 2017;90(22):199–209.
[31] Torquato S. Random heterogeneous materials: microstructure and macroscopic properties, 16. Springer Science & Business Media; 2013.
[32] Zillober C. A globally convergent version of the method of moving asymptotes. Structural optimization 1993;6(3):166–74.
[33] Coleman D, Holland P, Kaden N, Klema V, Peters SC. A system of subroutines for iteratively reweighted least squares computations. ACM Transactions on Mathematical Software (TOMS) 1980;6(3):327–36.
[34] Sobel I. An isotropic 3 $\times$3 image gradient operator. Machine vision for three-dimensional scenes 1990;37:6–379.
[35] Vincent OR, Folorunso O. A descriptive algorithm for sobel image edge detection, in: Proceedings of Informing Science & IT Education Conference (InSITE), 40, Informing Science Institute California, 2009, 97–107.
[36] Lee WB. Practical Application of Topology Optimization To the Design of Large Wind Turbine Towers. (MS (Master of Science) thesis), University of Iowa; 2015.